An XAS Investigation of the Nickel Site Structure in the Transcriptional Regulator InrS

Carolyn E. Carr,[1†] Andrew W. Foster,[3,4] and Michael J. Maroney*[1,2]

1Chemistry Department and *2Program in Molecular and Cellular Biology*, *University of Massachusetts Amherst, MA 01003, USA*; *3Department of Biosciences, Durham University, Durham, UK* and *4Department of Chemistry*, *Durham University, Durham*, *UK*.

*Corresponding Author: Michael J. Maroney, Department of Chemistry, Life Sciences Laboratory, Rm N373, 240 Thatcher Road, University of Massachusetts, Amherst, MA 01003-9336. Email: mmaroney@chem.umass.edu

Present Addresses:

[†]Department of Pharmaceutical Sciences, University of Nebraska Medical Center, 986025 Nebraska Medical Center, Omaha, Nebraska, 68198-6025, United States

ABSTRACT

InrS (Internal nickel-responsive Sensor) is a transcriptional repressor of the nickel exporter NrsD and de-represses expression of the exporter upon binding Ni(II) ions. Although a crystal structure of apo-InrS has been reported, no structure of the protein with metal ions bound is available. Herein we report the results of metal site structural investigations of Ni(II) and Cu(II) complexes of InrS using x-ray absorption spectroscopy (XAS) that are complementary to data available from the apo-InrS crystal structure, and are consistent with a planar four-coordinate [Ni(His)$_2$(Cys)$_2$] structure, where the ligands are derived from the side chains of His21, Cys53, His78, and Cys82. Coordination of Cu(II) to InrS forms a nearly identical planar four-coordinate complex that is consistent with a simple replacement of the Ni(II) center by Cu(II).

1. INTRODUCTION

InrS (Internal nickel-responsive Sensor) is a Ni(II)-responsive member of the RcnR-CsoR family of metalloregulators that is found in cyanobacteria (*Synechocystis sp*)[1]. It functions to de-repress the expression of a nickel exporter (NrsD) in response to high levels of intracellular Ni(II), and also enhances the expression of proteins involved in nickel import [1, 2]. InrS has a high affinity for Ni(II) (K_{metal} = 2.8 x 10^{-12} M), and Ni(II) binding is associated with a decrease in DNA affinity (apo InrS K_{DNA} ~ 9 x 10^{-9} M; Ni(II)-InrS K_{DNA} = 2.3 x 10^{-6} M)[3], which allows for the transcription of *nrsD*. *In vitro,* InrS binds many metals tightly and the change in DNA affinity is not metal-specific; Co(II), Cu(I) and Zn(II) are known to cause a decrease in InrS affinity for DNA[3]. In particular, Cu(II) is known to bind and to generate a similar decrease in DNA binding affinity to Ni(II) (Cu(II)-InrS K_{DNA} = 3.6 x 10^{-6} M)[2, 3]. The specificity of the biological response of a metalloregulator to nickel has been traced to a combination of the relative metal ion affinities of the ensemble of metalloregulators in the cell, relative allosteric efficacy of the metal ligand and the metal buffering capacity of the cytoplasm, which controls access to Ni(II)[2, 3].

Initial characterization of the Ni(II)-binding site in *Synechocystis* PCC 6803 InrS using electronic absorption spectroscopy indicated that the Ni(II) site was four-coordinate planar and featured at least one cysteine ligand[1]. Similar results were obtained for the Cu(II) complex [3]. Sequence alignments of the CsoR/RcnR family members reveal that the canonical W-X-Y-Z fingerprint, which denotes the spatial positions of the first coordination sphere residues of the metal-responsive members of this family of sensors [4, 5], corresponds to His21-Cys53-His78-Cys82 in InrS, where His21 aligns with His3 in *E. coli* RcnR [2, 6, 7], and Cys53-His78-Cys82 align with equivalent ligands in CsoR [2]. Studies employing mutagenesis confirm the roles of

Cys53-His78-Cys82 in Ni(II) binding [3]. Indeed, the crystal structure of apo-InrS subsequently revealed the proximity of Cys53-His78-Cys82, consistent with their role in the Ni(II) binding site[2]. However, no crystal structure of a metal complex of InrS exists. Although mutation of His21 leads to decreased Ni(II) affinity (K_{metal} = 5.5 x 10^{-11} M)[2], a role in metal coordination is somewhat obscured by the fact that there are six His residues in the N-terminal motif that contains this residue.

The purpose of this study is to provide a direct structural probe of the metal site in InrS in order to confirm the coordination number and geometry of the Ni(II) and Cu(II) complexes of InrS, to provide metric details of the metal site structures, and to provide insight into the role of His21 as the putative fourth Ni(II) binding ligand.

2. MATERIALS AND METHODS

2.1. Protein Samples

Synechocystis WT- and H21L-InrS were expressed and purified as previously described[1]. The concentrations of the metal stocks were verified by ICP-MS and metal complexes were prepared by adding 0.9 molar equivalents of $NiSO_4$ or $CuSO_4$ to solutions of purified proteins in 10 mM HEPES buffer, pH = 8.1, containing 1 M NaBr and 5 mM TCEP, which were then concentrated to 0.7-2.1 mM using a 10 kDa MWCO centrifugal concentrator. The samples were then loaded into polycarbonate sample holders with Kapton tape windows and frozen in liquid nitrogen.

2.2 XAS Data Collection

X-ray absorption spectroscopy (XAS) data were collected as previously described[8, 9] on beam line X3B at the National Synchrotron Light Source (NSLS), Brookhaven National

Laboratories (Upton, NY), except for Ni(II)-H21L, which used beam line 7-3 at the Stanford Synchrotron Radiation Laboratory (SSRL). Data collected at NSLS used samples that were cooled to ~30 K using a He displex cryostat and were collected under ring conditions of 2.8 GeV and 120-300 mA, with a sagittally-focusing Si(111) double-crystal monochromator. X-ray fluorescence was collected using a 30-element Ge detector (Canberra). Scattering was minimized by placing a Z-1 filter between the sample chamber and the detector. Internal energy calibration was performed by collecting spectra simultaneously in transition mode on the corresponding metal foil to determine the first inflection point on the edge, which was set to 8,331.6 (Ni(II)) or 8,980.3 eV (Cu(II)). X-ray absorption near-edge structure (XANES) data were collected from -200 to +200 eV relative to the metal K-edge. Extended X-ray absorption fine structure (EXAFS) data were collected to 15 k above the edge energy (E_0). Based on a >0.8 eV shift in edge energy between two successive scans, Cu(II)-InrS was photoreduced in the beam. To minimize the photoreduction, one batch of InrS was split into two samples, and each sample was moved after each scan so that the incident X-ray beam irradiated a new section of sample to obtain the spectrum of the Cu(II) complex. This method yielded 8 scans that were analyzed for differences in edge energies. No differences were observed in the 8 scans and these scans were averaged. Edges for the Cu(II) sample obtained in this fashion may be compared with a photoreduced sample (exposed until no further changes occurred) in the supporting information.

The Ni(II)-H21L sample was run on beam line 7-3 at SSRL. The data was collected at ~10 K using a liquid helium cryostat (Oxford Instruments) under ring conditions of 3 GeV and 495-500 mA. Beam line optics consisted of a Si(220) double-crystal monochromator and a flat rhodium-coated mirror before the monochromator for harmonic rejection and vertical collimation. X-ray

fluorescence was collected using a 30-element Ge detector (Canberra). Soller slits with a Z-1 element filter were placed between the sample chamber and the detector to minimize scattering.

2.3 XAS Data Analysis

The SixPack software[10] program was used to select the detector channels, average the data, and to perform energy calibration, data reduction and normalization. The Artemis software program was used for EXAFS analysis with parameters generated using FEFF6, which employs the IFEFFIT engine[11, 12]. Edge normalization was performed using a Gaussian pre-edge function and a quadratic polynomial for the post-edge region followed by normalization of the edge jump. A seven section fourth-order polynomial spline between $k = 2$ Å^{-1} and $k = 14$ Å^{-1} was used for EXAFS baseline correction. The data were converted to k-space using the $k = [\frac{2m_e(E-E_0)}{\hbar^2})]^{1/2}$ relationship. All data sets were Fourier-transformed using a Kaiser-Bessel window over the range $k = 2 - 14$ Å and fit in r-space over the range $r = 1 - 4$ Å in order to assess multiple-scattering contributions from histidine imidazole rings, and employing an amplitude reduction factor (S_0) value of 0.9. The reported Fourier-transformed spectra were not phase-corrected.

Reported data sets were first fit systematically for coordination numbers $4 - 6$, using all combinations of N and S scattering atom parameters with integer values of the number of scattering atoms within a shell of identical scattering atoms. The role of His imidazole ligands was then assessed by converting the N-donors to imidazole ligands (*vide infra*). Fits were also generated by refining the multiple S-donors in separate shells. The values of the metal-ligand distance, *r,* and disorder parameter, σ^2, were refined for each shell with different scattering atom types, (*i.e.,* the sulfur- and nitrogen-donors, the latter including imidazole rings). Each fit was initiated with a universal E_0 (8,340 eV for Ni(II) and 8,990 eV for Cu(II)) and $\Delta E_0 = 0$ eV, where

the value of ΔE_0 was allowed to vary for each fit. Histidine ligands were fit as geometrically rigid imidazole rings with varied angles of rotation (α), with α being defined as the rotation around an axis perpendicular to the plane of the ring and going through the coordinated nitrogen. The distances of the five non-hydrogen atoms in the imidazole ring were thus fit in terms of a single M-N distance for various angles of rotation ($\alpha = 0 - 10°$)[13-15]. Multiple-scattering parameters for imidazole ligands bound to Ni(II) and Cu(II) were generated using the FEFF6 software package with the imidazole input obtained from average bond lengths and angles gathered from crystallographic data, as previously described[8, 16]. Histidine "counting" was performed by adding integer numbers of His imidazole ligands to fits and assessing the effect on the R-factor and reduced χ^2 (*vide infra*).

The EXAFS was fit in Artemis using the standard EXAFS equation:

$$\chi(k) = \sum_i \frac{N_i f_i(k) e^{-2k^2 \sigma_i^2}}{k r_i^2} \sin[2k r_i + \delta_i(k)]$$

where *f(k)* is the scattering amplitude, *δ(k)* is the phase-shift, N is the number of identical neighboring atoms in a shell, r is the distance to these neighboring atoms, and σ^2 is the disorder to the nearest neighbors, summed over the number of shells, i.

To assess the goodness of fit from different fitting models, the fit parameters χ^2, reduced χ^2, and the R-factor were minimized. Increasing the number of adjustable parameters is generally expected to improve the R-factor; however χ^2 may go through a minimum, with the increase indicating the model is over-fitting the data. These parameters are defined as follows:

$$\chi^2 = \frac{N_{idp}}{N_{\varepsilon^2}} \sum_N^{i=1} (\{\text{Re}[\tilde{\chi}_{data}(R_i) - \tilde{\chi}_{theory}(R_i)]\}^2 + \{\text{Im}[\tilde{\chi}_{data}(R_i) - \tilde{\chi}_{theory}(R_i)]\}^2)$$

and

$$\text{reduced } \chi^2 = \frac{\chi^2}{N_{\text{idp}} - N_{\text{var}}}$$

where N_{idp} is the number of independent data points defined as $N_{\text{idp}} = \frac{(2\Delta r \Delta k)}{\pi}$, Δr is the fitting

range in r-space, Δk is the fitting range in k-space, N_{ε^2} is the number of uncertainties to

minimize, Re() is the real part of the EXAFS Fourier-transformed data and theoretical functions,

Im() is the imaginary part of the EXAFS Fourier-transformed data and theoretical functions, and

$\tilde{\chi}(R_i)$ is the Fourier-transformed data or theoretical function.

Additionally, IFEFFIT calculates the R-factor for each fit, which is directly proportional to χ^2

and is a measure of the absolute misfit between the data and theory given by:

$$R = \frac{\sum_{i=0}^{n}\left\{\left[\text{Re}\left[\tilde{\chi}_{\text{data}}(R_i) - \tilde{\chi}_{\text{theory}}(R_i)\right]\right\}^2 + \left\{\text{Im}(\tilde{\chi}_{\text{data}}(R_i)) - \tilde{\chi}_{\text{theory}}(R_i)\right]\right\}^2\right)}{\sum_{i=0}^{n}\left\{\left[\text{Re}(\tilde{\chi}_{\text{data}}(R_i))\right]^2 + \left[\text{Im}(\tilde{\chi}_{\text{data}}(R_i))\right]^2\right\}}$$

3. RESULTS

3.1 XANES Analysis

The analysis of the x-ray absorption near-edge spectrum (XANES) yields information

regarding the coordination number and geometry of the metal center. XANES data for the Ni(II)-

and Cu(II)-complexes of InrS samples are shown in **Figure 1** and the analyses are summarized in

Tables 1 and **2**. All of the XANES spectra lack an obvious pre-edge peak associated with a 1s $\rightarrow$

3d transition, and so the intensity of this feature is near zero ($< 0.5 \times 10^{-2}$). For the Ni(II)

complexes of WT- and H21L-InrS, this indicates a centrosymmetric arrangement of ligands in

both cases, and is consistent with either a four-coordinate planar or six-coordinate geometry[17].

The spectrum of Ni(II) WT-InrS also exhibits a resolved maximum at ~8,336 eV, which is associated with a 1s → 4p$_z$ transition and is diagnostic for a four-coordinate planar geometry, thus ruling out a six-coordinate site[17]. This feature is also observed for the Ni(II) complex of H21L-InrS, confirming the four-coordinate planar geometry of both Ni(II) complexes. However, the XANES spectra of the two Ni(II) complexes are not identical, indicating that the Ni(II) site is structurally perturbed in the H21L-InrS variant.

As noted above, the Cu(II) complex of InrS is photoreduced in the beam. Efforts were made to minimize photoreduction by exposing a fresh portion of the sample on each scan (see Sec. 2.2). The resulting averaged spectrum reveals a relatively featureless Cu K-edge. In general, the Cu(II) pre-edge region is often featureless and is notably insensitive to changes in ligand environment, making assignment of the coordination number/geometry from XANES analysis difficult and often impossible [18-20]. The Cu(II)-InrS complex does not exhibit a pre-edge feature associated with a 1s → 3d transition. This feature is often absent, particularly in the case of planar Cu(II) species [21], because of decreased intensity due to the d^9 electronic configuration, but the low intensity is consistent with a centrosymmetric geometry. The Cu(II)-InrS spectrum does exhibit a low-energy pre-edge tail with a normalized amplitude of 0.39 at 8384.0 eV that arises from a shoulder near 8986 eV that is associated with a 1s → 4p transition. The presence and intensity of this feature is indicative of higher covalency in the Cu(II) site, and in biologically relevant complexes is only observed in complexes that contain two or more S-donor ligands [18, 22].

3.2 EXAFS Analysis

Analysis of the extended x-ray absorption fine structure (EXAFS) region of an XAS spectrum yields information regarding the types of donor atoms (Z ± 2) in the primary

coordination sphere and their distance from the scattering atom (± 0.02 Å), as well as providing a second measure of the coordination number (± ~20 %). Because EXAFS fitting cannot differentiate between atom types with Z ± 1, it can be difficult to distinguish protein S-donor ligands from Cl⁻ ligands derived from buffers containing NaCl. For this reason the EXAFS data was collected using buffers containing NaBr.

Analysis of the data began by examining the first coordination sphere by evaluating models with coordination numbers 4 – 6 with all possible combinations of N- or S- donors and by incorporating potential Br⁻ ligands. The best EXAFS fits (**Table 1, Figure 2**) obtained for the Ni(II) WT-InrS spectrum are four-coordinate, consistent with the XANES analysis, and feature two N/O-donors and two S-donor ligands. In addition to peaks arising from these scattering atoms in the first coordination sphere (**Figure 2**, $r \sim 1.5 - 2.2$ Å, uncorrected for phase shifts), the Fourier-transformed data for Ni(II) WT-InrS shows several peaks arising from scattering atoms at distances corresponding to the second and third coordination spheres of the Ni(II) center (**Figure 2**, $r \sim 2.5 - 4.0$ Å, uncorrected for phase shifts) that in biological samples suggest the presence of histidine imidazole ligands. When the N/O-donors were modeled as rigid imidazole rings with multiple-scattering parameters, the best fit indicated that both N/O-donors could be fit as histidine ligands. In fact, an acceptable fit of the data (one with $R < 5\%$) could not be obtained without including multiple-scattering from two imidazole rings. The fit featuring coordination of two imidazoles decreased the %R value by almost half relative to a fit with only one imidazole ring while also improving value of reduced χ^2, and resulted in two Ni-N(His) distances of 1.87(1) Å and 2.02(2)Å (**Table 1**). These distances are in the range expected for four-coordinate planar Ni(II) sites, and the difference in the distances is larger than the resolution of the data set ($k = \frac{\pi}{2 \times \Delta k} = 0.126$ Å), and therefore consistent with the coordination of two

histidine ligands at distinct distances. The analysis of the S-donors in the Ni(II) WT-InrS site was done with either a single shell of two S-scattering atoms, or by refining the two Ni(II)-S distances independently (**Table 1**). The latter approach led to one short (2.15(3) Å) and one longer Ni(II)-S distance (2.25(2) Å), the shorter of which is near the lower limit observed for four-coordinate planar thiolates[23]. However, the difference in the two Ni-S distances is below the resolution of the data set (*vide supra*). Refinement as one shell of two S-donors fits nearly as well, and results in a reasonable average Ni(II)-S distance for a four-coordinate planar complex (2.23(1) Å). Combined with the results of the XANES analysis indicating a four-coordinate planar Ni(II) site, the EXAFS results are consistent with a planar [Ni(His)$_2$(Cys)$_2$] complex in WT-InrS.

Visual inspection of the region in the Fourier-transformed spectrum that corresponds to multiple-scattering (**Figure 2;** $r \sim 2.4 - 4$ Å) reveals that the best fit does not adequately account for all the features seen. By varying the distance and type of ligands and angle of the imidazole rings, all possible variations of the fit involving imidazole ligands were tried, but no better fit was obtained. This indicates that our model is not accounting for some features at ~3 - 4 Å. There are a number of potential scattering atoms at longer distances that are not included in a model featuring only first coordination sphere donors and imidazole rings, and scattering pathways involving these atoms likely account for the observation of the additional features.

A similar analysis of the EXAFS arising from the Cu(II) WT-InrS metal site gives analogous results (**Table 2**). For the Cu(II) site, inclusion of multiple-scattering from imidazole rings is not required in order to generate a fit with %R < 5%, however inclusion of multiple-scattering pathways for imidazole ligands improves both the %R and the reduced χ^2 values, with the model where both N/O donors are imidazole ligands being slightly better that the model with one

imidazole. Splitting the S shell into two shells also improves the fits slightly, with the Cu-S distances obtained (2.19 and 2.30 Å) but the difference is again below the resolution of the data (*vide supra*). The average Cu-S distance obtained from fitting both S-donors as a single shell is 2.25(1) Å, which is within experimental error of the range reported for planar Cu(II) complexes (2.26 – 2.32 Å)[24, 25] Overall, the M-L distances obtained from the EXAFS analysis (**Table 2**) are appropriate for a planar four-coordinate [Cu(II)(His)$_2$(Cys)$_2$] complex, and the results are fully consistent with Cu(II) occupying the same site as Ni(II) in WT-InrS.

The EXAFS analysis of the Ni(II) H21L-InrS complex shows the nature of the structural perturbation of the Ni(II) site seen in the XANES spectra (**Table 1**). Like the Ni(II) WT-InrS complex, the site was best modeled by two N/O-donors and two S-donors, and an acceptable fit could not be generated without including multiple-scattering from an imidazole ligand. However, in contrast to the WT-InrS Ni(II) site, modeling both N/O-donors as imidazole ligands did not improve the fit. The best fits were obtained when the S-donors were refined independently. These fits gave two Ni-S distances that are close to the resolution of the data (Ni-S = 2.12 and 2.24 Å), and the fit with a single histidine imidazole was superior to the one with two imidazole ligands--a result that is consistent with H21 providing the second imidazole ligand in WT-InrS. Addition of a second imidazole ring raises both the *R*-factor and the value of reduced χ^2, albeit by modest amounts compared to the differences in these parameters for the one and two imidazole fits of the Ni(II) WT-InrS data. The more modest changes in the fit parameters may arise from partial substitution of H21 by other His imidazole side-chains in H21L-InrS, since the N-terminal motif containing H21 has several other histidine residues, including neighboring His19.

In a similar vein to WT-InrS complexed to Ni(II), there is a notable mismatch between the data and the best fit in the multiple-scattering region ($r \sim 2.5 - 4$ Å) of the Fourier-transformed data in **Figure 2**. This would again suggest that whatever long-range interactions that are visible in the WT-InrS data, but not included in the model, are also present in the mutant.

4. DISCUSSION

The XAS analysis presented provides compelling evidence for a planar [Ni(His)$_2$(Cys)$_2$] site in WT-InrS. The identity of the ligands involved can be inferred from mutational analysis on the effect of Ni(II) binding[3], sequence homologies with other proteins in the CsoR/RcnR family of DNA-binding proteins[2 , 6, 7], and the crystal structure of apo-InrS[2], which shows that Cys53 from subunit A and His78 and Cys82 from subunit B of the tetrameric protein are located together in the structure, forming a metal binding site (**Figure 3**). The four-coordinate planar arrangement found for the ligands in the Ni(II) complex and the position of His78 between the two Cys ligands in the crystal structure of apo-InrS indicates that the *trans*-[M(His)$_2$(Cys)$_2$] isomer is likely formed in the Ni(II) and Cu(II) complexes.

The identity of the fourth ligand, the second His ligand, is less clear. Sequence homology indicates that His21 corresponds to His3 in the *E. coli* RcnR sequence, which is essential for metal-responsiveness and is a ligand in the RcnR Co(II) complex, but not for the Ni(II) complex[7]. Further, His21 is remote from the Cys53-His78-Cys82 ligands in the Ni(II) site in the apo-InrS structure (the distance between His21 Cα and His78 Cα is 11.9 Å in chain B), but does lie in the flexible N-terminal motif of the protein that could allow it bind to the Ni(II) center, as is typical of metal binding in other members of the RcnR/CsoR family of metalloregulators [2, 5, 26]. The XANES data presented for the H21L-InrS Ni(II) complex show

that mutation of His21 leads to a structural perturbation in the Ni(II) site. Given its remote location in the crystal structure of the apo-InrS, this result indicates a role for H21 in the Ni(II) site structure. EXAFS analysis shows that in contrast to the spectra obtained for WT-InrS, where Ni(II) is clearly bound to two His imidazole ligands, the data for H21L-InrS is better fit by a model featuring only one His ligand and an unknown N/O-donor, possibly water derived from the buffer. In combination, these results provide an indication of the structural role of His21 in the InrS metal binding site.

The analysis of XANES and EXAFS data for the Cu(II) complex of WT-InrS is consistent with a straight-forward substitution of Cu(II) for Ni(II), resulting in an analogous planar four-coordinate $trans$-[Cu(His)$_2$(Cys)$_2$] site. Complexes of Cu(II) normally adopt a Jahn-Teller distorted "4+2" six-coordinate structure, which is ruled out by the XAS analysis. The overall neutral charge on the [Cu(His)$_2$(Cys)$_2$] complex, coupled with any protein steric restraints, is apparently sufficient to eliminate axial ligation. Since Cu(II) apparently binds to InrS using the same ligands and in the same geometry as Ni(II), it is not surprising that InrS also responds to Cu(II) binding in $vitro$. This result provides further structural validation for the use of Cu(II) as a surrogate for Ni(II) in in $vitro$ studies of metal binding and allosteric response[2].

The four-coordinate planar structure of the WT-InrS Ni(II) site contrasts with the six-coordinate Ni(II) structure found in another Ni(II)-responsive transcriptional regulator in the CsoR/RcnR family, namely $E.$ $coli$ RcnR[6], which controls the de-repression of the expression of the export proteins RcnAB in response to Ni(II) or Co(II) binding. RcnR features a six-coordinate site involving ligation by the N-terminal amine, a single Cys residue--Cys35, Glu63, His64, and at least one other N/O-donor ligand [7, 27]. Because all known four-coordinate planar Ni(II) complexes have a low-spin (S = 0) electronic configuration, and all six-coordinate Ni(II)

complexes are high-spin (S = 1), the differences between the Ni(II) sites in these two transcriptional regulators have important implications for the structure and function of the two sites. The ramifications of the difference in electronic structure between InrS and RcnR can be seen in the structure of the two Ni(II) sites. The Ni-S distances found for InrS (2.23(1) Å) are vastly different than the single Ni-S distance reported for *E. coli* RcnR (2.54 Å) [6]. With respect to metal recognition, since a planar four-coordinate geometry is common only for d^8 Ni(II) among first row transition metals, it is easier to envision InrS being able to discriminate between metals based on coordination number and geometry than is RcnR, since all first-row transition metals form six-coordinate complexes. Indeed, RcnR also responds to Co(II) *in vivo*, which also forms a six-coordinate complex. However, studies of the coordination environment of Ni(II) and Co(II) in RcnR indicate that the coordination number/geometry does not play a major role in the allosteric response of this protein [27].

The structure of the InrS Ni(II) site resembles aspects of other nickel protein complexes including another transcriptional regulator, NikR[28, 29], and the enzyme NiSOD[30, 31]. NikR represses the transcription of the NikABCDE Ni(II)-specific importer in response to binding Ni(II) [32]. This transcriptional regulator belongs to the ribbon-helix-helix family of DNA-binding proteins[32] and contains a planar four-coordinate [Ni(His)$_3$(Cys)] high-affinity Ni(II) site that features a very short Ni-S distance of 2.13(1)Å[33], but is similar to the shorter of the two Ni-S bonds found for the InrS complex, and three Ni-N bonds that average 1.91 Å, similar to the average of the two Ni-N(His) bonds in the InrS Ni(II) site (1.95 Å).

The structures of the nickel-reponsive transcriptional regulators NikR and RcnR are distinguished from InrS and other protein nickel sites by the use of a single Cys ligand. Nickel enzymes that catalyze biological redox reactions involving the Ni(III/II) couple feature two or

more S-donor ligands [34-36]. The active site of NiSOD in the Ni(II) oxidation state is an example of the latter and features planar four-coordinate ligation of the nickel center by two N-donors (the N-terminal amine and the Cys2 amidate) and two Cys S-donors in a *cis*-geometry, with Ni-S distances of ~2.15 Å[37], also similar to the Ni-S distance determined for the InrS Ni(II) site. NiSOD is a redox enzyme that catalyzes the disproportionation of superoxide anion using a ping-pong mechanism that employs the Ni(II/III) redox couple. The Cys ligands in the NiSOD active site have been shown to be primarily responsible for lowering the redox potential of the Ni(II/III) couple into a biologically accessible range, ~ 290 mV [36, 38, 39]. This indicates that InrS should be capable of supporting Ni(III/II) redox chemistry at a potential that is biologically accessible, while the nickel sites found in the other transcriptional regulators should not.

5. CONCLUSIONS

The analyses of Ni and Cu K-edge XANES and EXAFS data from the Ni-responsive transcriptional regulator InrS have provided structural details of this novel metal site. The data obtained on the WT-InrS Ni(II) site provide compelling evidence for a four coordinate planar [Ni(His)$_2$(Cys)$_2$] complex. Given the prior information available from amino acid sequence analysis, mutagenesis and the crystal structure of apo-InrS, three of the ligands were identified as Cys53-His78-Cys82, and are constrained in a way that the *trans*-isomer is favored. Data obtained on the H21L-InrS variant support the identification of His21 as the fourth ligand in the metal binding site, consistent with amino acid sequence alignments between InrS and other members of the RcnR/CsoR family of DNA-binding proteins. XAS data obtained for the Cu(II)-substituted

WT-InrS complex is consistent with maintenance of the Ni(II) ligand environment and geometry, and also consistent with the fact that InrS responds to Cu(II)-binding *in vitro*.

ABBREVIATIONS

CsoR   *Copper-sensing operon repressor*

Cys   *Cysteine*

DNA   *Deoxyribonucleic acid*

EXAFS   *Extended x-ray absorption fine structure*

HEPES   *4-(2-hydroxyethyl)-1-piperazineethanesulfonic acid*

His   *Histidine*

Im   *Imidazole*

InrS   *Internal Nickel-Responsive Sensor*

MWCO   *Molecular weight cut-off*

NikR   *Nickel import regulator*

NiSOD   *Nickel-dependent superoxide dismutase*

nrs   *Nickel response operon*

RcnR   *Resistance to cobalt and nickel repressor*

TCEP   *tris(2-carboxyethyl)phosphine*

XANES   *x-ray absorption near-edge structure*

XAS   *x-ray absorption spectroscopy*

ACKNOWLEDGMENTS

ASSOCIATED CONTENT

Supporting Information. Figure S1 comparing the Cu K-edge XANES spectrum obtained from fresh sample and the photoreduction product.

REFERENCES

[1] A.W. Foster, C.J. Patterson, R. Pernil, C.R. Hess, N.J. Robinson J. Biol. Chem. 287 (2012) 12142-12151.

[2] A.W. Foster, R. Pernil, C.J. Patterson, A.J.P. Scott, L.O. Palsson, R. Pal, I. Cummins, P.T. Chivers, E. Pohl, N.J. Robinson Nat. Chem. Biol. 13 (2017) 409-414.

[3] A.W. Foster, R. Pernil, C.J. Patterson, N.J. Robinson Mol. Microbiol. 92 (2014) 797-812

[4] K.A. Higgins, D. Giedroc Chem. Lett. 43 (2014) 20-25.

[5] F.-M.J. Chang, H.J. Coyne, C. Cubillas, P. Vinuesa, X. Fang, Z. Ma, D. Ma, J.D. Helmann, A. Garcia-de los Santos, Y.-X. Wang, C.E. Dann, D.P. Giedroc J. Biol. Chem. 289 (2014) 19204-19217.

[6] J.S. Iwig, S. Leitch, R.W. Herbst, M.J. Maroney, P.T. Chivers J. Am. Chem. Soc. 130 (2008) 7592-7606.

[7] K.A. Higgins, P.T. Chivers, M.J. Maroney J. Am. Chem. Soc. 134 (2012) 7081-7093

[8] V. Martin-Diaconescu, M. Bellucci, F. Musiani, S. Ciurli, M.J. Maroney J. Biol. Inorg. Chem. 17 (2012) 353-361.

[9] J. Dong, C.A. Joseph, N.B. Borotto, V.L. Gill, M.J. Maroney, R.W. Vachet Biochemistry 53 (2014) 1263-1274.

[10] S.M. Webb Physica Scripta T115 (2005) 1011-1014.

[11] B. Ravel, M. Newville J. Synchrotron Radiat. 12 (2005) 537-541.

[12] M. Newville J. Synchrotron Radiat. 8 (2001) 322-324.

[13] N.J. Blackburn, S.S. Hasnain, T.M. Pettingill, R.W. Strange J. Biol. Chem. 266 (1991) 23120-23127.

[14] G.C. Ferreira, R. Franco, A. Mangravita, G.N. George Biochemistry 41 (2002) 4809-4818.

[15] K. Banaszak, V. Martin-Diaconescu, M. Bellucci, B. Zambelli, W. Rypniewski, M.J. Maroney, S. Ciurli Biochem. J. 441 (2012) 1017-1026.

[16] R.A. Engh, R. Huber Acta Crystallogr. A 47 (1991) 392-400.

[17] G.J. Colpas, M.J. Maroney, C. Bagyinka, M. Kumar, W.S. Willis, S.L. Suib, P.K. Mascharak, N. Baidya Inorg. Chem. 30 (1991) 920-928.

[18] L.S. Kau, D.J. Spira-Solomon, J.E. Penner-Hahn, K.O. Hodgson, E.I. Solomon J. Am. Chem. Soc. 109 (1987) 6433-6442.

[19] R. Sarangi Coord. Chem. Rev. 257 (2013) 459-472.

[20] J.L. DuBois, P. Mukherjee, A.M. Collier, J.M. Mayer, E.I. Solomon, B. Hedman, T.D.P. Stack, K.O. Hodgson J. Am. Chem. Soc. 119 (1997) 8578-8579.

[21] M. Sano, S. Komorita, H. Yamatera Inorg. Chem. 31 (1992) 459-463.

[22] K. Clark, J.E. Penner-Hahn, M.M. Whittaker, J.W. Whittaker J. Am. Chem. Soc. 112 (1990) 6433-6434.

[23] H.J. Krueger, R.H. Holm Inorg. Chem. 28 (1989) 1148-1155.

[24] T.D. Tullius, P. Frank, K.O. Hodgson Proc. Natl. Acad. Sci. USA 75 (1978) 4069-4073.

[25] R.A. Scott, S.P. Cramer, R.W. Shaw, H. Beinert, H.B. Gray Proc. Natl. Acad. Sci. USA 78 (1981) 664-667.

[26] K.J. Denby, Iwig, J., Bisson, C., Westwood J., Rolfe, M. D., Sedelnikova, S. E., Higgins, K., Maroney, M. J., Baker, P. J., Chivers, P. T., and Green, J. Sci. Rep. 6 (2016).

[27] C.E. Carr, F. Musiani, H.-T. Huang, P.T. Chivers, S. Ciurli, M.J. Maroney Inorg. Chem. 56 (2017) 6459-6476.

[28] E.R. Schreiter, Sintchak, M. D., Guo, Y., Chivers, P. T., Sauer, R. T., Drennan, C. L. Nat. Struct. Biol. 10 (2003) 794-799.

[29] P.T. Chivers, T.H. Tahirov J. Mol. Biol. 348 (2005) 597-607.

[30] D.P. Barondeau, C.J. Kassmann, C.K. Bruns, J.A. Tainer, E.D. Getzoff Biochemistry 43 (2004) 8038-8047.

[31] J. Wuerges, J.W. Lee, Y.I. Yim, H.S. Yim, S.O. Kang, K.D. Carugo Proc. Natl. Acad. Sci. USA 101 (2004) 8569-8574.

[32] P.T. Chivers, R.T. Sauer Protein Sci. 8 (1999) 2494-2500.

[33] S. Leitch, M.J. Bradley, J.L. Rowe, P.T. Chivers, M.J. Maroney J. Am. Chem. Soc. 129 (2007) 5085-5095.

[34] W. Lubitz, H. Ogata, O. Rudiger, E. Reijerse Chemical Revs. 114 (2014) 4081-4148.

[35] M. Can, F.A. Armstrong, S.W. Ragsdale Chemical Revs. 114 (2014) 4149-4174.

[36] J.O. Campeciño, M.J. Maroney, in: D. Zamble, M. Rowinska-Zyrek, H. Kozlowski (Eds.), The Biological Chemistry of Nickel, vol. Metallobiology Series No.10, The Royal Society of Chemistry, 2017, pp. 170-199.

[37] S.B. Choudhury, J.-W. Lee, G. Davidson, Y.-I. Yim, K. Bose, M.L. Sharma, S.-O. Kang, D.E. Cabelli, M.J. Maroney Biochemistry 38 (1999) 3744-3752.

[38] R.W. Herbst, A. Guce, P.A. Bryngelson, K.A. Higgins, K.C. Ryan, D.E. Cabelli, S.C. Garman, M.J. Maroney Biochemistry 48 (2009) 3354-3369.

[39] A.T. Fiedler, P.A. Bryngelson, M.J. Maroney, T.C. Brunold J. Am. Chem. Soc. 127 (2005) 5449-5462.

Table 1. XANES and EXAFS Analysis for Nickel Complexes of WT- and H21L-InrS.*

	XANES Analysis				EXAFS Analysis					
Sample	K-edge energy (eV)	$1s \rightarrow 3d$ peak area (x10^2 eV)	$1s \rightarrow 4p_z$ observed	Coord.#/ geometry	Shell	r (Å)	σ^2 (x10^{-3} Å^2)	ΔE_0 (eV)	%R	Red.χ^2
WT	8341.5	<0.5	Yes	4/planar	2 N/O	1.89(3)	7(3)	-3(2)	14.3	67.5
					2 S	2.21(1)	4(1)			
					1 N/O	1.86(2)	2(2)	0(2)	9.3	49.5
					2 S	2.22(1)	5(1)			
					1 Im 0°	1.98(5)	5(4)			
					2 S	**2.23(1)**	**5(1)**	**2(1)**	**4.9**	**23.1**
					1 Im 0°	**2.02(2)**	**1(1)**			
					1 Im 0°	**1.87(1)**	**1(1)**			
					1 N/O	1.87(3)	2(2)	0(3)	8.9	54.2
					1 S	2.18(3)	1(2)			
					1 S	2.28(3)	2(3)			
					1 Im 0°	1.96(6)	6(7)			
					1 S	2.18(4)	7(6)	0(2)	4.3	25.9
					1 S	2.26(3)	2(2)			
					1 Im 0°	2.02(2)	1(1)			
					1 Im 0°	1.87(1)	1(1)			
H21L	8342.3	<0.5	Yes	4/planar	2 N/O	1.89(1)	4(1)	-1(2)	9.4	95.3
					2 S	2.21(1)	3(0)			
					1 N/O	1.84(3)	3(3)	-3(1)	5.0	57.0
					2 S	2.20(1)	3(0)			
					1 Im 0°	1.90(2)	1(1)			
					2 S	2.21(1)	3(1)	-1(2)	5.0	56.3
					1 Im 0°	1.87(1)	0(2)			
					1 Im 0°	1.98(4)	3(5)			
					1 N/O	**1.86(2)**	**1(1)**	**-1(2)**	**4.1**	**54.0**
					1 S	**2.12(2)**	**3(4)**			
					1 S	**2.24(1)**	**1(1)**			
					1 Im 10°	**2.02(2)**	**1(1)**			
					1 S	2.22(2)	0(1)	-2(2)	4.7	61.0
					1 S	2.16(4)	7(7)			
					1 Im 0°	1.86(2)	0(2)			
					1 Im 0°	1.99(3)	1(3)			

*Fits shown in **bold** type are shown in Figure 2. Numbers in parenthesis represent estimated uncertainties in refined parameters and represent the change in the variable that will result in an increase in χ^2 of 1. The data for Ni(II) WT-InrS lacks the resolution in the data to split the sulfur shells. These fits have been included for comparison to the H21L-InrS fit.

Table 2. XANES and EXAFS Analysis for the Cu(II) Complex of WT-InrS.*

	XANES Analysis				EXAFS Analysis					
Sample	K-edge energy (eV)	1s → 3d peak area (x10^2 eV)	1s → 4p$_z$ observed	Coord.#/ geometry	Shell	r (Å)	σ^2 (x10^{-3} Å^2)	ΔE_0 (eV)	%R	Red.χ^2
WT	8990.0	<0.5	Yes	4/planar	2 N/O 2 S	2.09((2) 2.27(1)	5(2) 6(1)	7(2)	4.0	11.6
					1 N/O 2 S 1 Im 0°	2.07(3) 2.26(1) 2.02(5)	3(2) 6(1) 10(6)	2(2)	3.4	11.1
					2 S 1 Im 0° 1 Im 0°	2.25(1) 2.06(6) 2.06(14)	5(1) 6(6) 13(16)	1(2)	3.1	10.3
					1 N/O 1 S 1 S 1 Im 0°	2.08(4) 2.16(3) 2.29(2) 2.01(3)	2(2) 5(10) 1(2) 5(3)	1(2)	2.6	2.6
					1 S **1 S** **1 Im 0°** **1 Im 10°**	**2.19(1)** **2.30(1)** **1.99(3)** **2.14(2)**	**0(1)** **1(1)** **7(3)** **3(2)**	**0(1)**	**1.8**	**6.7**

*Fits shown in **bold** type are shown in Figure 2. Numbers in parenthesis represent estimated uncertainties in refined parameters and represent the change in the variable that will result in an increase in χ^2 of 1. The Cu(II) WT-InrS data lacks sufficient resolution to split the sulfur shells. These fits have been included for comparison to H21L-InrS.

Figure Captions

Figure 1. *K*-edge XANES spectra of InrS Ni(II) complexes (top) and the WT-InrS Cu(II) complex (bottom) in buffer containing 10 mM HEPES pH = 8.1, 1 M NaBr and 5 mM TCEP.

Figure 2. Left: Fourier-transformed K-edge EXAFS spectra (colored lines) and fits (black lines) from Tables 1 and 2 of Ni(II) WT- (top) and H21L-InrS (middle) and Cu(II) WT-InrS (bottom) complexes in buffer containing 10 mM HEPES pH = 8.1, 1 M NaBr and 5 mM TCEP. Right: Corresponding unfiltered k^3-weighted EXAFS spectra and fits.

Figure 3. Ribbon Diagram of apo-InrS showing the positions of the Ni(II) ligands His21, Cys53, His78, and Cys82 (PDB 5FMN).

Figure 1
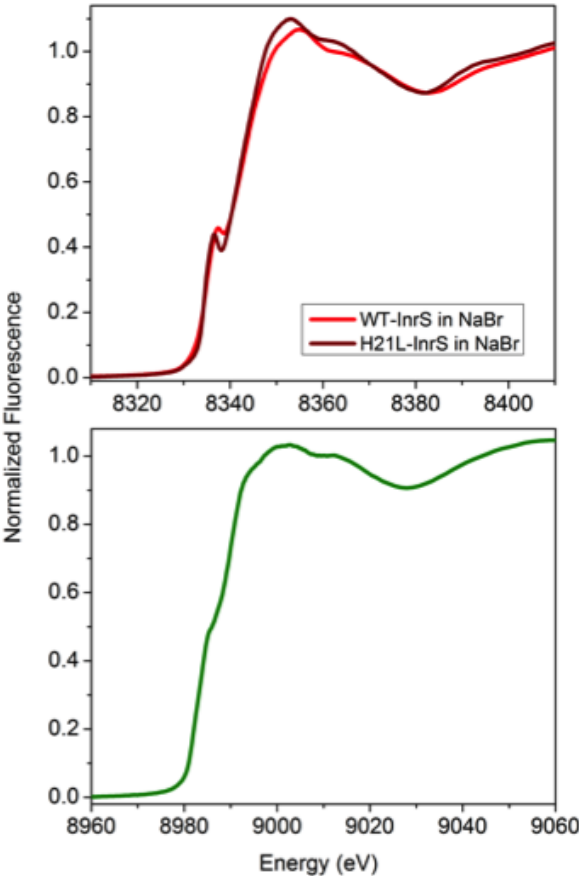
Figure 2
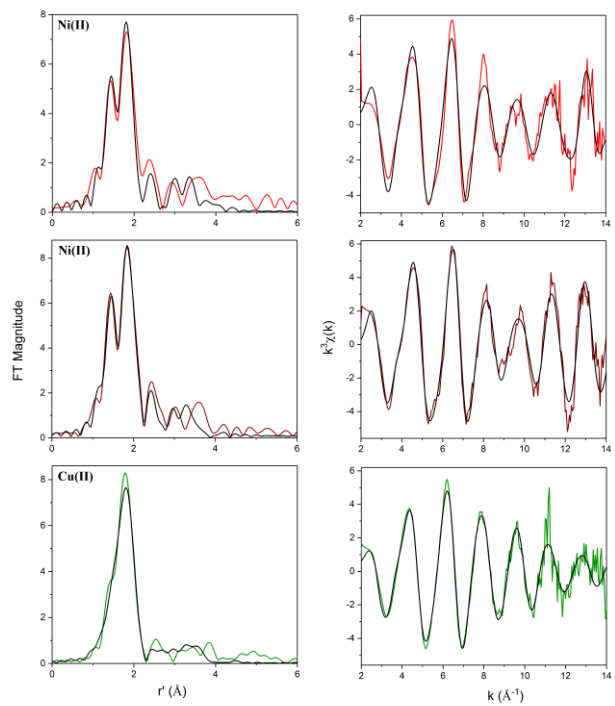
Figure 3
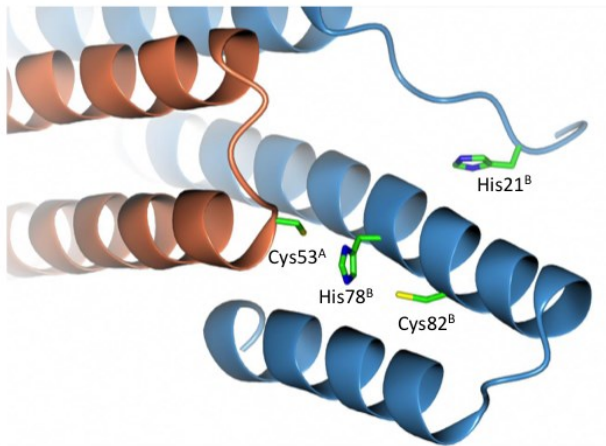
Graphical Abstract
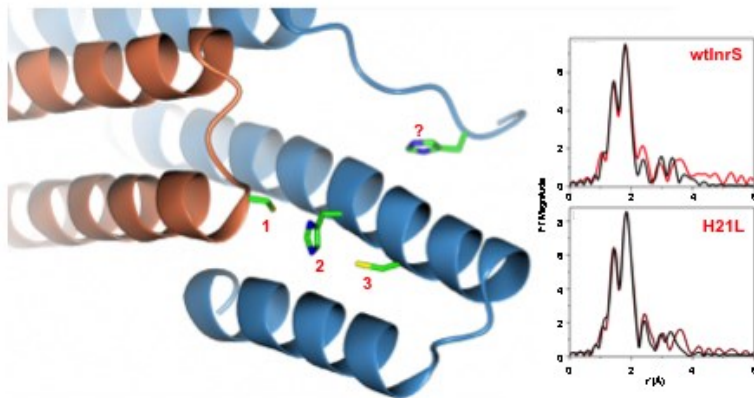
InrS (Internal Nickel-Responsive Sensor) is a nickel-responsive transcriptional repressor. We report metal site structural investigations of Ni(II) and Cu(II) complexes of InrS using x-ray absorption spectroscopy (XAS) that are complementary to data available from the apo-InrS crystal structure, and are consistent with a planar four-coordinate $[M(His)_2(Cys)_2]$ metal binding site.